EDGE ARTICLE

Check for updates

All publication charges for this article have been paid for by the Royal Society of Chemistry

Construction of a homologous series of metal nanoclusters and implications for structure–activity correlations

Qinzhen Li, †[ab] Tingting Jiang,†[b] Sha Yang, [b] Jinsong Chai, *[ab] Haizhu Yu *[b] and Manzhou Zhu *[b]

The precise structures of metal nanoclusters (NCs) can serve as an accurate model for the establishment of a structure–activity correlation, thereby attracting attention as a new type of heterogeneous catalyst. However, it remains challenging to definitively establish the relationship between the structure of local sites on NCs and catalytic activity. Herein, a homologous series of metal NCs were constructed for the structure–activity correlation. Four NCs including $Au_{24}(SAdm)_{14}(OPDP)_1$ (**Au$_{24}$**), $Au_{23}Cd_1(SR)_{14}(OPDP)_1Cl$ (**Au$_{23}$Cd$_1$**), $Au_{22}Cd_2(SAdm)_{14}(OPDP)_1Cl_2$ (**Au$_{22}$Cd$_2$**) and $Au_{21}Cd_2(SAdm)_{13}(OPDP)_1Cl_2$ (**Au$_{21}$Cd$_2$**) (HSAdm = 1-adamantanethiol; OPDP = (oxydi-2,1-phenylene)bis(diphenylphosphine)) were synthesized. These four NCs exhibit the same common $Au_{21}M_1(SR)_{10}(OPDP)_1$ (M = Au/Cd) structural skeleton but two different surface motifs. These two motifs in the four NCs exhibit regular evolution mode, that is, $2[Au_1(SR)_2]$ for **Au$_{24}$**, $[Au_1(SR)_2] + [Cd_1(SR)_3Cl]$ for **Au$_{23}$Cd$_1$**, $2[Cd_1(SR)_3Cl]$ for **Au$_{22}$Cd$_2$**, and $[Cd_1(SR)_3Cl] + [CdCl]$ for **Au$_{21}$Cd$_2$**. The electrocatalytic oxygen reduction reaction (ORR) is performed with these four NCs as catalysts, revealing a catalytic activity sequence of **Au$_{21}$Cd$_2$** > **Au$_{22}$Cd$_2$** > **Au$_{23}$Cd$_1$** > **Au$_{24}$**. Based on the differences in surface motifs, the structure–activity relationship can be rigorously correlated with certain motif types, showing an activity sequence of $[CdCl] > [Cd_1(SR)_3Cl] > [Au_1(SR)_2]$. Moreover, compared with the other three NCs, **Au$_{21}$Cd$_2$** showed a higher electron transfer number and a smaller Tafel slope in catalyzing the ORR, indicating a different kinetic reaction process and higher reactivity of [CdCl] than $[Cd_1(SR)_3Cl]$ and $[Au_1(SR)_2]$, which revealed a configuration effect in determining catalytic activity of NCs.

Introduction

As important catalytically active materials in the field of nanocatalysis, metal nanoparticle catalysts have received extensive attention because they present the advantages of high turnover in homogeneous catalysis and recyclability in heterogeneous catalysis.[1–3] Understanding the catalytic mechanism and revealing the structure–activity relationship are of great significance for their performance improvement, upgrading and iteration.[4–6] Relevant mechanism studies have shown that specific local structural sites of metal nanoparticles, such as crystal facets and defects,[7,8] play a decisive role in determining the catalytic activity, but due to the difficulties in the precise structural characterization of the active site, more detailed mechanism discovery and the establishment of accurate structure–activity relationships are still challenging.

Nanoclusters (NCs) have shown unique advantages in correlating structure–activity because their precise structures can serve as an accurate research model for the mechanism study and avoid the error caused by the structure simulation.[9–15] Nevertheless, the structural diversity among NCs (including differences in metal cores, surface motifs, and ligand types)[16–19] greatly reduces their structural comparability, making it difficult to accurately correlate their structure–activity relationships. In this regard, NCs that bear a single structural variable were singled out to construct comparable systems and simplify the research models for structure–activity correlations. For the metal core part, size-dependent activity was revealed by comparing the catalytic effect between Au NCs with different sizes (Scheme 1a).[20–24] Moreover, with the construction of alloyed counterparts from the same parent NC, the doping effect on catalytic activity can be well elucidated,[25,26] which can even reach the level of single atoms (Scheme 1b).[27–31] On the other hand, the ligand effect on the catalytic activity has also been investigated by changing the ligand type on the surface of certain NCs (Scheme 1c).[32–36] However, surface motifs (or local sites) of NCs are regarded as an important origin of their

School of Materials Science and Engineering, Anhui University, Hefei, Anhui 230601, China. E-mail: chaijs@ahu.edu.cn

Department of Chemistry and Centre for Atomic Engineering of Advanced Materials, Key Laboratory of Structure and Functional Regulation of Hybrid Materials of Ministry of Education, Institutes of Physical Science and Information Technology and Anhui Province Key Laboratory of Chemistry for Inorganic/Organic Hybrid Functionalized Materials, Anhui University, Hefei, Anhui 230601, China. E-mail: yuhaizhu@ahu.edu.cn; zmz@ahu.edu.cn

† These authors contributed equally to this work.

a) *Size effect*

b) *Doping effect*

Doping type

Doping degree
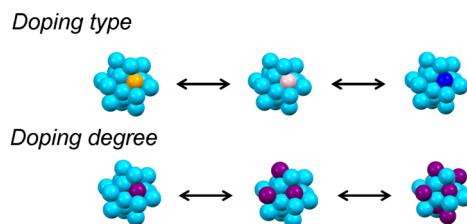
c) *Ligand effect*

- -
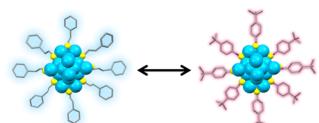
d) *This work: Structure effect from local sites*

Au₂₄ **Au₂₃Cd₁** **Au₂₂Cd₂** **Au₂₁Cd₂**
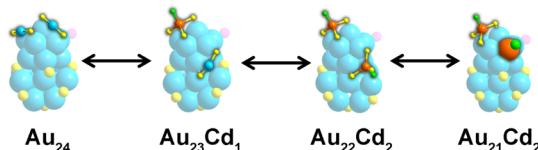
Scheme 1 Schematic representation of NC series for investigating the structure–activity relationship: (a) NCs with different sizes; (b) NCs doped with different types (or numbers) of heterometal atoms; (c) NCs protected by different types of ligands; (d) NCs with the same skeleton but different local motifs.

catalytic activity,[37–39] and the configuration effect of NCs on catalytic activity has not been systematically studied due to the difficulty in constructing NC series bearing only differences in the configuration of local sites.

Heterometal doping is a widely used implementation strategy to regulate the molecular compositions of the parent NCs.[40–45] Among the common heterometal types for doping parent Au NCs, Cd has shown great potential in regulating the local structure of NCs due to the diversity of its doping modes in Au NCs. Cd can be doped into different parts of the NCs, including the surface motif, core surface and core center,[46] which allows it to construct specific Cd-doping sites in NCs with distinct structural configurations. More importantly, the introduction of Cd atoms can achieve local structural regulation while maintaining the basic skeleton of the parent Au NCs.[47–49] In addition to this, the as-introduced Cd atoms in Au NCs can serve as active sites for further catalytic reactions,[47,50,51] which will be beneficial to the study of its structure–activity relationship. Inspired by this, we expect to obtain a series of structural analogues by controlling the doping process of Cd atoms in Au NCs, so as to establish an accurate structure–activity relationship by correlating their structural and performance differences.

Herein, taking a newly synthesized $Au_{24}(SAdm)_{14}(OPDP)_1$ (Au_{24}, HSAdm = 1-adamantanethiol; OPDP = (oxydi-2,1-

phenylene)bis(diphenylphosphine)) as parent NC, three Au–Cd alloy NCs were constructed via a controlled stepwise Cd-doping process, formulated as $Au_{23}Cd_1(SAdm)_{14}(OPDP)_1Cl$ ($Au_{23}Cd_1$), $Au_{22}Cd_2(SAdm)_{14}(OPDP)_1Cl_2$ ($Au_{22}Cd_2$), and $Au_{21}Cd_2(SAdm)_{13}(OPDP)_1Cl_2$ ($Au_{21}Cd_2$), respectively. Single crystal X-ray diffraction (SC-XRD) reveals that these three Au–Cd NCs exhibit a high degree of structural homology with Au_{24} and show significant structural continuity (Scheme 1d). That is, all four NCs exhibit the same $Au_{21}M_1(SR)_{10}(OPDP)_1$ (M = Au/Cd) structural skeleton, which is composed of a $Au_{15}M_1$ kernel, two $Au_1(SR)_2$, one bridged SR, one $Au_4(SR)_5$, and one OPDP ligand. Anchored on this common skeleton, the remaining two surface motifs in these four NCs show regular evolution, that is, two $Au_1(SR)_2$ for Au_{24}, one $Au_1(SR)_2$ and one $Cd_1(SR)_3Cl$ for $Au_{23}Cd_1$, two $Cd_1(SR)_3Cl$ for $Au_{22}Cd_2$, and one $Cd_1(SR)_3Cl$ and one CdCl for $Au_{21}Cd_2$. Taking these four nanocluster homologues as a research platform, the relationship between the oxygen reduction reaction (ORR) electrocatalytic activity and precise structure was established unambiguously, which demonstrated a configuration effect of the local sites on catalytic activity, that is a catalytic activity sequence of $[CdCl] > [Cd_1(SR)_3Cl] > [Au_1(SR)_2]$.

Results and discussion

As the parent Au NC for constructing structural homologues, Au_{24} was synthesized via a two-phase ligand exchange method.[52] Pure Au_{24} can be obtained by separating the raw product with a thin-layer chromatography plate. UV-vis spectroscopy showed a series of characteristic peaks located at 343, 364, 391, 452, 494, 582, 678, and 750 nm, respectively (Fig. 1a). Electrospray mass spectrometry (ESI-MS) in positive mode showed an intense signal at 3803.3 Da (Fig. 1b), which can be assigned to the formula $Au_{24}(SAdm)_{14}(OPDP)_1$ bearing +2 charge (calculated position: 3803.3 Da). The well-matched isotopic pattern between experimental and calculated data further supports this molecular composition. The atomically precise structure is the key information necessary to study the structural evolution of NCs. So, X-ray single crystal diffraction was employed to figure out its molecular structure. Au_{24} crystallizes in the monoclinic $P2_1/c$ group with four NCs in one unit cell (Fig. 1a, inset; Table S1). Au_{24} was revealed to exhibit a Au_{16} kernel, which can be regarded as a combination of one icosahedral Au_{13} and one tetrahedral Au_4 by sharing a vertex atom. As shown in Fig. 1c, the icosahedron and tetrahedral unit in the kernel were connected by one bridging thiolate and two $Au_1(SR)_2$ motifs and one $Au_4(SR)_5$ was found to bind on the bottom of the icosahedral Au_{13} unit and surround the Au_4 unit. Furthermore, two more $Au_1(SR)_2$ and one diphosphine ligand were anchored on the top side of the Au_{16} kernel, forming the complete Au_{24} NCs.

$CdCl_2$ was first reacted with Au_{24} to induce the Cd-doping process. However, no new species were generated in this reaction, instead, Au_{24} was decomposed in 6 h (Fig. S1). A further attempt via reacting Au_{24} with both $CdCl_2$ and HSAdm successfully triggered the doping process, and a $Au_{23}Cd_1$ NC can be isolated. Its crystal structure (reported in our previous work)[46] is similar to that of the parent Au_{24} NCs, and they bear
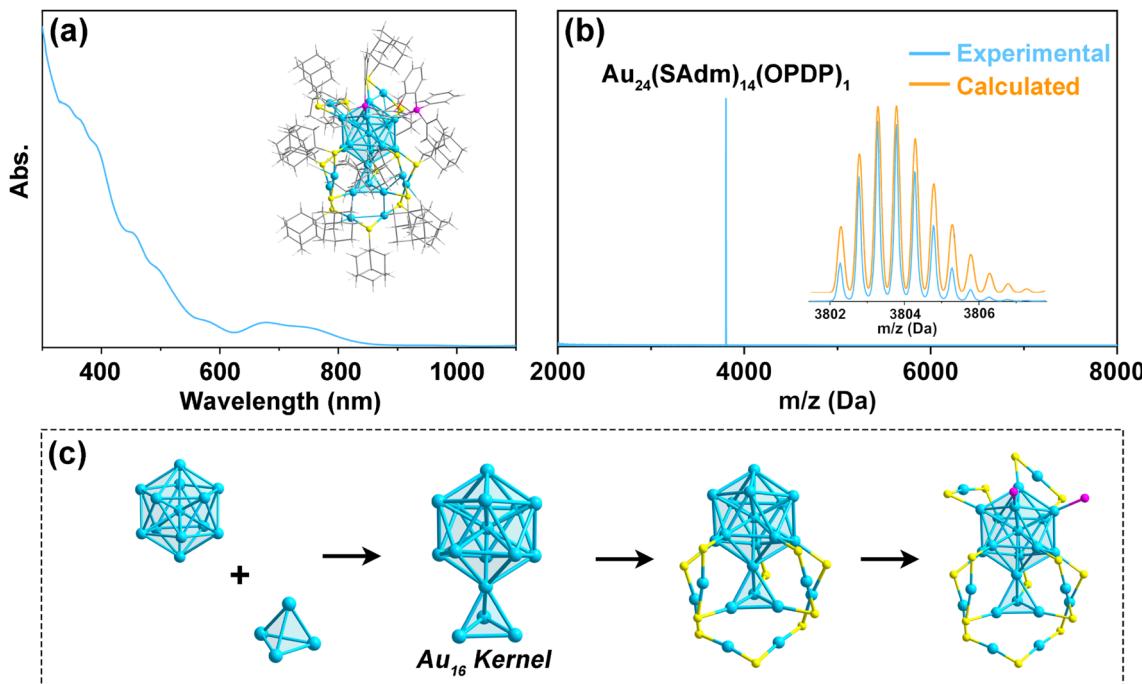
Fig. 1 (a) UV-vis spectrum of Au_{24}. Inset: total structure of Au_{24}. (b) ESI-MS of Au_{24}. Inset: experimental and calculated isotopic patterns of the MS signal. (c) Structural analysis of the skeleton in Au_{24}. (Labels: light blue = Au; yellow = S; magenta = P; gray = C; red = O; white = H).

the same structural skeleton. Besides, they show differences in the motifs located on the top of the Au_{16} kernel, at which the two $Au_1(SR)_2$ in Au_{24} were reconstructed as one $Cd_1(SR)_3Cl$ and one new $Au_1(SR)_2$ in $Au_{23}Cd_1$ (Fig. S2). The structural

transformation from Au_{24} into $Au_{23}Cd_1$ was investigated using time-dependent UV-vis spectroscopy and ESI-MS (Fig. 2I). Time-dependent UV-vis spectroscopy revealed a gradual attenuation of the characteristic peak belonging to Au_{24} and a set of new
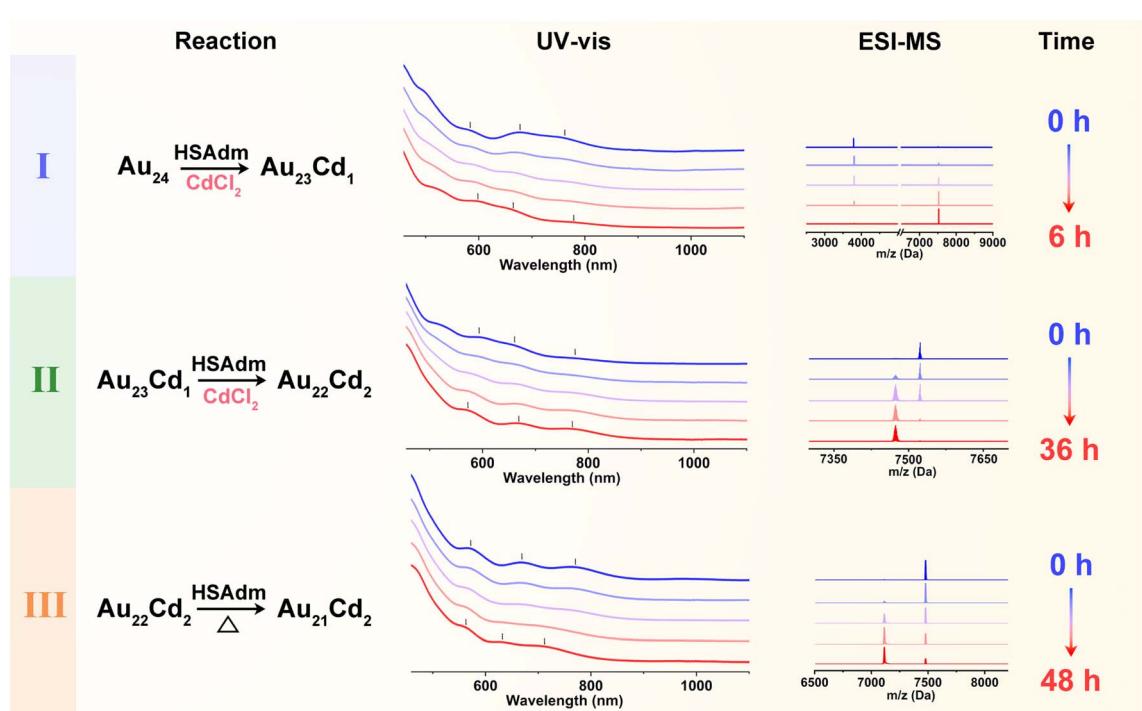

Fig. 2 Reaction system composition and the time-dependent UV-vis spectra and ESI-MS of the three transformation stages, including Au_{24} to $Au_{23}Cd_1$ (stage I), $Au_{23}Cd_1$ to $Au_{22}Cd_2$ (stage II), and $Au_{22}Cd_2$ to $Au_{21}Cd_2$ (stage III).

peaks located at 520, 600, 650, and ∼770 nm emerged. At the same time, changes in the reaction components were also monitored by ESI-MS. The results showed that, along with the weakening of the **Au₂₄** signal, a peak located at 7522.5 Da belonging to $[Au_{23}Cd_1(SAdm)_{14}(OPDP)_1]^+$ gradually increased. These observations demonstrated that the **Au₂₄** can be converted into **Au₂₃Cd₁** by introducing Cd species. After 6 h, the signal of **Au₂₄** became invisible, indicating that **Au₂₄** has been completely converted.

Interestingly, after all **Au₂₄** were converted to **Au₂₃Cd₁**, it was found that further extension of the reaction time would result in the formation of another new species, showing a signal located at 7473.5 Da in ESI-MS (Fig. S3). Considering that the addition of CdCl₂ (20 equivalents of **Au₂₄**) in the reaction is excessive, this phenomenon may suggest that **Au₂₃Cd₁** is not the final state of the reaction, and it can continue to undergo structural transformation. Based on this conjecture, **Au₂₃Cd₁** was isolated and purified as the reactant to mix with CdCl₂ and HSAdm. As a result, time-dependent UV-vis spectroscopy revealed a transformation in absorption peaks from that of **Au₂₃Cd₁** to three new peaks located at 560, 660 and 760 nm. Further ESI-MS analysis revealed a newly emerged signal at 7473.5 Da and the reaction ended after about 36 h. This signal peak matched well with the formula $[Au_{22}Cd_2(SAdm)_{14}(OPDP)_1Cl]^+$, indicating the additional doping of another Cd atom in the **Au₂₃Cd₁** NCs (Fig. 2II).

The acquisition of **Au₂₂Cd₂** motivated us to investigate whether it could further undergo a structural transformation process. Therefore, **Au₂₂Cd₂** was treated with the same reaction conditions as those for **Au₂₄** and **Au₂₃Cd₁**; however, **Au₂₂Cd₂** remained unchanged under these conditions. It was noted that

the reaction rate from **Au₂₃Cd₁** to **Au₂₂Cd₂** slowed down significantly compared with the reaction from **Au₂₄** to **Au₂₃Cd₁** (36 h *vs.* 6 h), implying that the reaction between **Au₂₂Cd₂** and Cd might be more difficult. So, the reaction temperature was elevated to promote any possible transformation process. At a reaction temperature of 55 °C, it was found that **Au₂₂Cd₂** can slowly transform into another species. Time-dependent UV-vis spectroscopy showed a blue shift in the absorption peaks and ESI-MS revealed that the newly formed NCs exhibited a signal peak located at 7109.5 Da (Fig. 2III). This peak position corresponds to the molecular formula of $[Au_{21}Cd_2(SAdm)_{13}(OPDP)_1Cl]^+$. In this case, the doping number of Cd atoms did not change from **Au₂₂Cd₂** to **Au₂₁Cd₂**, indicating that it is not a doping process. Thus, we removed the CdCl₂ from the reaction and found that the transformation can still happen. The transformation from **Au₂₂Cd₂** into **Au₂₁Cd₂** showed a quite low reaction rate and there will be some untransformed **Au₂₂Cd₂** in the final system. A further attempt to trigger the structural transformation of **Au₂₁Cd₂** with Cd-doping or heat treatment did not yield any new species (Fig. S4), demonstrating that **Au₂₁Cd₂** was a stable product that can be regarded as the final state of this entire transformation pathway (**Au₂₄** → **Au₂₃Cd₁** → **Au₂₂Cd₂** → **Au₂₁Cd₂**). This process can also be observed clearly by thin-layer chromatography separation (Fig. S5).

To unravel the structural relationship between these NCs, the atomically precise structures of the other two NCs, **Au₂₂Cd₂** and **Au₂₁Cd₂**, were solved with SC-XRD (Tables S2 and 3). Interestingly, all four NCs including **Au₂₄**, **Au₂₃Cd₁** **Au₂₂Cd₂** and **Au₂₁Cd₂** were revealed to exhibit a high degree of structural homology. As shown in Fig. 3, all four NCs exhibit an Au₁₅M₁ (M = Au/Cd) kernel protected by one Au₄(SR)₅, one bridging
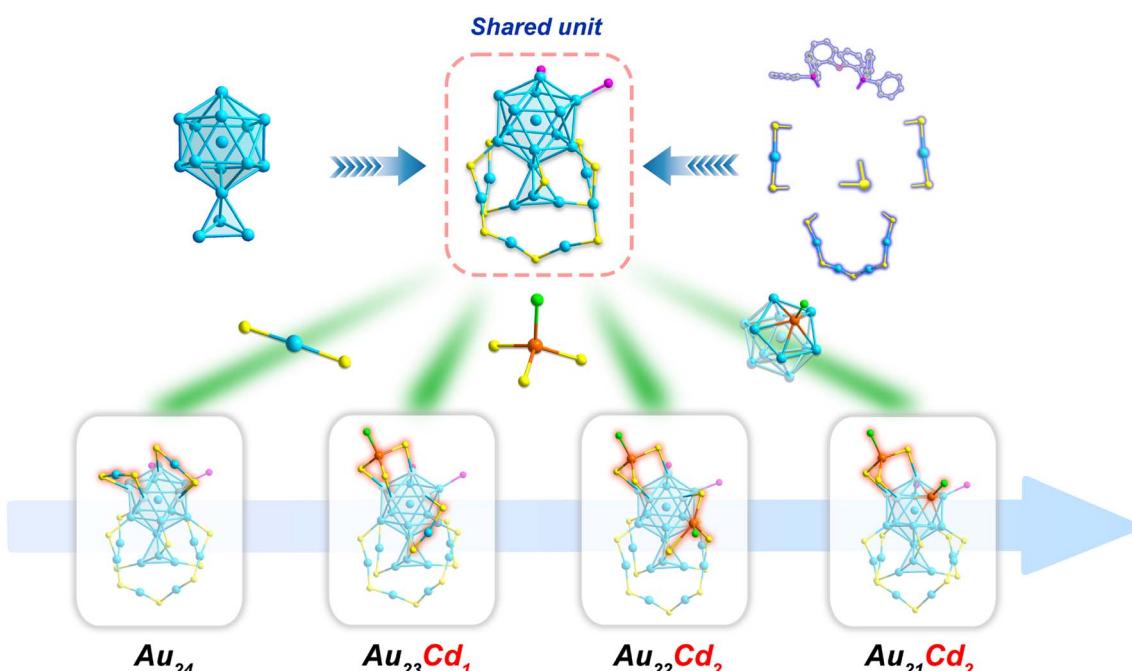
Fig. 3 Illustration of the shared structural unit in Au₂₄, Au₂₃Cd₁, Au₂₂Cd₂ and Au₂₁Cd₂, and the movement trajectory of Cd atoms in NCs as the doping process progresses. (Labels: light blue = Au; orange = Cd; bright green = Cl; yellow = S; magenta = P; gray = C; red = O).

thiolate, one diphosphine and two $Au_1(SR)_2$ with the same binding site. Apart from this shared structure unit, there are four binding sites left on the surface of the $Au_{15}M_1$ kernel, and structural differences of these four NCs were found to exist in these positions. For Au_{24}, two adjacent $Au_1(SR)_2$ motifs were found to bind on these four remaining coordination sites. After the doping of one Cd atom in Au_{24}, $Au_{23}Cd_1$ was formed and the motifs at this site change into a $Cd_1(SR)_3Cl$ unit and a new $Au_1(SR)_2$. Further doping of Cd resulted in the formation of two $Cd_1(SR)_3Cl$ motifs in $Au_{22}Cd_2$. Finally, in $Au_{21}Cd_2$, one of the Cd atoms collapses into the core surface, forming a $Au_{15}Cd_1$ kernel with the configuration maintained, and one $Cd_1(SR)_3Cl$ and one Cl were anchored on those four binding sites. UV-vis spectra and ESI-MS of $Au_{23}Cd_1$, $Au_{22}Cd_2$, and $Au_{21}Cd_2$ solution obtained by dissolving their crystal samples were subsequently recorded, which revealed consistent absorption peaks and formula (Fig. S6) with the previous results (Fig. 2) and crystal structures.

To understand the role of Cd in constructing structure homologues, the reaction system (containing Au_{24}, $CdCl_2$ and HSAdm initially) was analyzed by mass spectrometry to clarify the existence form of the introduced Cd element and the removed gold atom. For the initial state, a significant signal peak belonging to the $[CdCl]^+$ species was detected in the reaction system. After the transformation from Au_{24} into $Au_{23}Cd_1$, $Au_1(SR)_2^-$ can be found in the reaction solution (Fig. S7). This result indicated that $[CdCl]^+$ was an important species to trigger the doping process, while the substituted gold atom was generated in the form of $Au_1(SR)_2^-$. The capture of $Au_1(SR)_2^-$ species explains why the thiolate ligand is necessary for triggering the structural conversion, that is, thiolate ligands act as a stabilizer for the substituted gold atoms, thus facilitating the reaction.

DFT calculations were then employed to reveal the pathway throughout the entire structural transformation process with a ligand-simplified model (Fig. S8).[53] Given that the $Au_1(SR)_2$ motif in Au_{24} will convert into a $Cd_1(SR)_3Cl$ motif in $Au_{23}Cd_1$, two possible pathways that can achieve this motif transition, that is, a $Au_1(SR)_2$ motif infusion process and a $[CdCl]$ substitution process were considered. As shown in Fig. S9, the energy barrier of these two processes was calculated, respectively. The result showed that the $[CdCl]$ substitution process was a more energetically favorable process, demonstrating that the replacement of a Au atom by a $[CdCl]$ unit is the triggering step of the transformation from Au_{24} into $Au_{23}Cd_1$. The calculated pathway indicated $[CdCl]$ insertion and $Au_1(SR)_2$ rearrangement processes (Fig. S10a and S11). The second stage, from $Au_{23}Cd_1$ to $Au_{22}Cd_2$ can be achieved in one step by the substitution of a Au atom with a $[CdCl]$ unit (Fig. S10b). As shown in Fig. S12, the spatial position of two SR from $Au_1(SR)_2$ and one SR from $Au_4(SR)_5$ together form a suitable doping site for the construction of a $Cd_1(SR)_3Cl$ motif in tetrahedral geometry. The existence of this special site may be the key to facilitate the Cd-doping reaction. In the third stage, $Au_{22}Cd_2$ was found to transform into the final product $Au_{21}Cd_2$ *via* undergoing two intermediate states (Fig. S10c). In the first step, the $[CdCl]$ unit of the $Cd_1(SR)_3Cl$ motif in $Au_{22}Cd_2$ collapses downward into the

surface of the Au_{13} icosahedral unit in the kernel, forming the $Au_{13}Cd_1$ core unit. This $Au_{13}Cd_1$ intermediate state then reverts to the $Au_{12}Cd_1$ icosahedron with the extrusion of one Au atom, forming the final $Au_{21}Cd_2$ NCs. This calculated result is consistent with the fact that $Au_{22}Cd_2$ can be converted into $Au_{21}Cd_2$ without the addition of an extra Cd source.

That is, with the combination of the atomically precise structures and calculated transformation pathway, the evolutionary rule for this homologous series of NCs can be summarized as two continuous processes: the gradual increase in Cd doping number and the outward to inward transfer of the Cd substitution site, which is manifested as the gradual replacement of $Au_1(SR)_2$ by $Cd_1(SR)_3Cl$ motifs, and the subsequent collapse of $Cd_1(SR)_3Cl$ into the core-anchored CdCl unit.

The structural similarity allows these nanocluster homologues to serve as a unique research platform for studying and establishing their structure–activity correlation while excluding the influence of size and ligand effects. As shown in Fig. S13, all four NCs display similar absorption characteristics within the short-wavelength region (<450 nm), which is attributed to their similar kernel structures, and the differences in their motifs primarily affect the positions of absorption peaks at long wavelengths. Then, their photoluminescence properties were also evaluated. As shown in Fig. S14, only Au_{24} exhibits weak near-infrared photoluminescence at ∼1000 nm while the other three NCs do not exhibit photoluminescence performance.

Furthermore, electrocatalytic ORR activity was evaluated using the four NCs as catalysts (Fig. 4a and S15). All four NCs were loaded on the activated carbon as the electrocatalysts (Fig. S16) and the ORR tests were performed with these four electrocatalysts under the same conditions. As shown in Fig. 4a, the current density displayed a gradually increasing trend with a sequence of $Au_{24} < Au_{23}Cd_1 < Au_{22}Cd_2 < Au_{21}Cd_2$.

The acquisition of the precise structures of these four nanocluster homologues allows us to accurately correlate their structure–activity relationships based on their local structural differences. The ORR current density for Au_{24} and $Au_{23}Cd_1$ was revealed to be 2.55 and 3.17 mA cm^{-2} (0.17 V, 1600 rpm), respectively. Given that their only structural difference lies in two surface motifs, that is, Au_{24} has two $Au_1(SR)_2$ while $Au_{23}Cd_1$ exhibits one $Cd_1(SR)_3Cl$ and one $Au_1(SR)_2$, one can easily draw the conclusion that the newly formed $Cd_1(SR)_3Cl$ motif in $Au_{23}Cd_1$ can serve as a more active catalytic site in the ORR than the $Au_1(SR)_2$ motif. In addition, $Au_{22}Cd_2$ (with two $Cd_1(SR)_3Cl$ motifs on the surface) displays a current density of 3.47 mA cm^{-2} under the same conditions, showing a slight enhancement in the catalytic activity when compared with that of $Au_{23}Cd_1$ (bearing one $Cd_1(SR)_3Cl$), indicating that the as-formed second $Cd_1(SR)_3Cl$ unit in $Au_{22}Cd_2$ can improve the catalytic performance to some extent by increasing the active sites. Furthermore, a more significant change in current density can be observed for $Au_{21}Cd_2$ (4.22 mA cm^{-2}). Since there is only one structural difference between $Au_{22}Cd_2$ and $Au_{21}Cd_2$, that is, a $Cd_1(SR)_3Cl$ motif of $Au_{22}Cd_2$ changes into a CdCl unit that collapsed in the kernel in $Au_{21}Cd_2$, this result demonstrated that the enhanced catalytic activity for $Au_{21}Cd_2$ can be attributed to this change in the doping position and configuration of
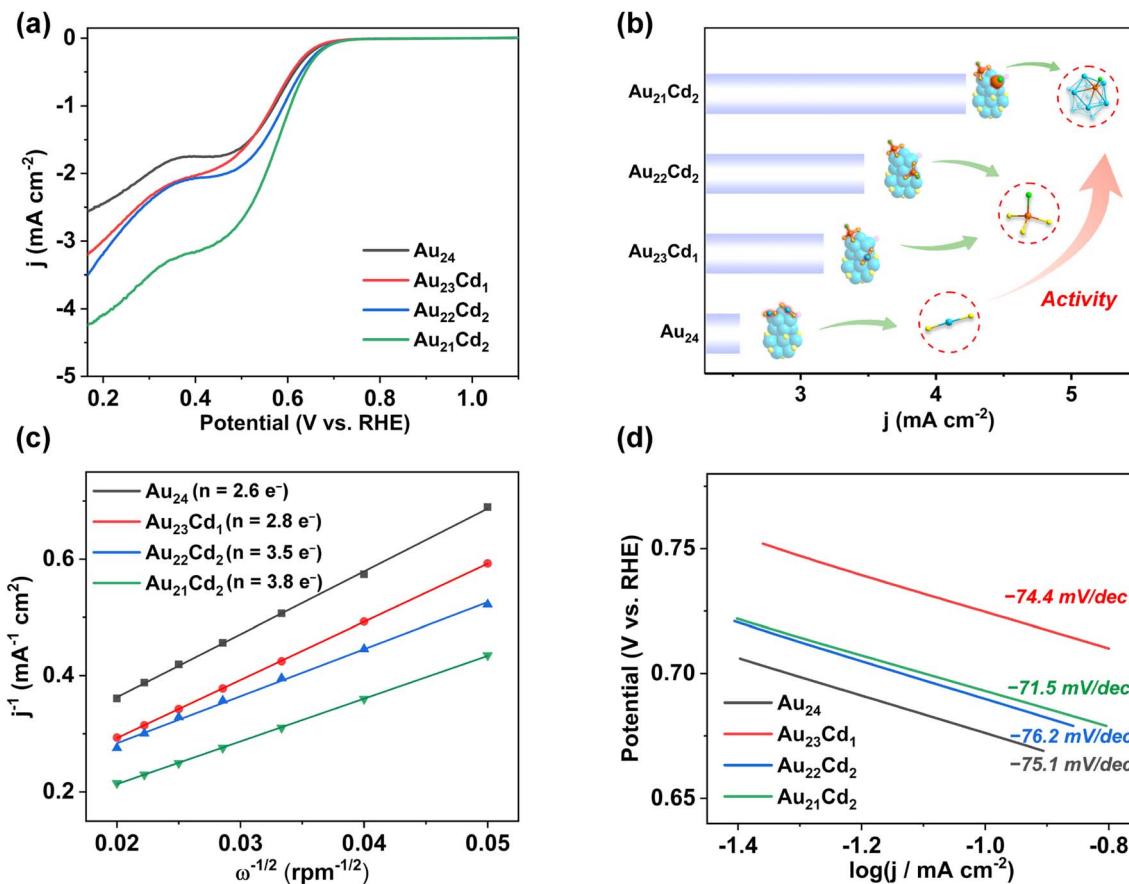
Fig. 4 (a) ORR polarization curves for different NCs as catalysts obtained in O_2-saturated 0.1 mol per L KOH solutions at 1600 rpm. (b) The current density values for different NCs as catalysts (0.17 V, 1600 rpm) and the corresponding different local structures of these NCs. (c) Koutecky–Levich plots (j^{-1} vs. $\omega^{-1/2}$) of different NCs. (d) Corresponding Tafel plots of the NCs.

the Cd atom. That is, the catalytic activity sequence was clearly revealed as [CdCl] > [Cd$_1$(SR)$_3$Cl] > [Au$_1$(SR)$_2$] (Fig. 4b). This shows that the Cd-containing structural sites are more active than the Au-containing unit, which was probably caused by breaking of the Cd–Cl bond than can expose the coordination site for the combination between the Cd atom and substrate molecule. As evidence, the dissociation of Cl atoms can be observed in all the ESI-MS results of the three Au–Cd NCs (**Au$_{23}$Cd$_1$, Au$_{22}$Cd$_2$** and **Au$_{21}$Cd$_2$**) in this work (Fig. S6). After the removal of a Cl atom from CdCl and Cd$_1$(SR)$_3$Cl, the active sites for these two cases are the icosahedral Au$_{12}$Cd$_1$ and the Cd$_1$(SR)$_3$ unit, respectively. Considering the higher stability of the icosahedral structure, it will be more conducive to the dissociation of the Cl atom and the removal of the product molecule from the active sites during catalysis, thus explaining the higher catalytic activity of CdCl than Cd$_1$(SR)$_3$Cl.

More importantly, the transformation of local configurations of active sites from Cd$_1$(SR)$_3$Cl into CdCl shows a significant effect on catalytic activity. The overall transferred electrons were calculated according to the Koutecky–Levich plots (Fig. 4c), demonstrating equivalent ORR electron transfer numbers of n = 2.6, 2.8, and 3.5 for **Au$_{24}$, Au$_{23}$Cd$_1$,** and **Au$_{22}$Cd$_2$**, respectively. This indicates that **Au$_{24}$, Au$_{23}$Cd$_1$,** and **Au$_{22}$Cd$_2$** reduced O_2 through a combination of 2 e$^-$ and 4 e$^-$ processes. An electron

transfer number of n = 3.8 e$^-$ was revealed for **Au$_{21}$Cd$_2$**, indicating a dominant four-electron reduction process for it. This indicated that the incorporation of Cd in **Au$_{24}$** can change the reaction mechanism from a 2 e$^-$ to a 4 e$^-$ process and the core-doping type of Cd in **Au$_{21}$Cd$_2$** shows the most remarkable effect. Besides, Tafel plots revealed similar slope values for **Au$_{24}$, Au$_{23}$Cd$_1$,** and **Au$_{22}$Cd$_2$** at ~75 mV per dec, while a smaller slope value (71.5 mV per dec) for **Au$_{21}$Cd$_2$** is observed (Fig. 4d), demonstrating a higher kinetic reaction rate for the CdCl unit in it. The above results unambiguously demonstrated that changing the configuration of the active site in the NCs is a powerful means to enhance the catalytic activity by changing the kinetics and reaction mechanism of the catalytic reaction.

Conclusions

In this study, a homologous series of metal NCs including **Au$_{24}$, Au$_{23}$Cd$_1$, Au$_{22}$Cd$_2$** and **Au$_{21}$Cd$_2$**, was constructed via a controlled stepwise Cd-doping process. These four NCs differ from each other in structure by only two surface motifs. Structural analysis revealed a regular structural evolution pattern in these NCs, which showed the gradual conversion from Au$_1$(SR)$_2$ to Cd$_1$(SR)$_3$Cl motifs, and finally the CdCl unit inserting in the icosahedral kernel. The structure continuity of this set of nanocluster

structure homologues was further used to study the relationship between its local sites and the catalytic performance. An ORR catalytic activity sequence of $Au_{24} < Au_{23}Cd_1 < Au_{22}Cd_2 < Au_{21}Cd_2$ was revealed. By combining the catalytic results and the precise structures of NCs, the structure–activity relationship was unambiguously revealed, showing an activity sequence of $[CdCl] > [Cd_1(SR)_3Cl] > [Au_1(SR)_2]$ in local structural sites. In addition, Koutecky–Levich and Tafel plots demonstrated that the as-formed [CdCl] unit in $Au_{21}Cd_2$ can lead to a dominant four-electron reduction pathway and smaller Tafel slope when compared with the other three NCs, showing the important role of the structural configuration in local sites in determining the reaction mechanism and kinetics for nanocluster catalysts. This work has systematically studied the relationship between the surface configuration of local sites and catalytic activity through the construction of nanocluster structure homologues, which offers a new perspective for the study of structure–activity relationships in NCs.

Author contributions

All authors have given approval to the final version of the manuscript. Q. L. executed the experimental synthesis, characterization, and data analysis. T. J. and H. Y. carried out the theoretical calculations. Q. L. carried out single-crystal X-ray diffraction data collection and structure refinement; Q. L., T. J. and S. Y. prepared the first draft of the manuscript and all authors contributed to the preparation of the manuscript. J. C., H. Y., and M. Z. supervised the project.

Conflicts of interest

There are no conflicts to declare.

Data availability

CCDC 2374164, 2128986 and 2341165 contain the supplementary crystallographic data for this paper.[54a–c]

The data supporting this article have been included as part of the SI. Supplementary information: supporting figures, and tables. See DOI: https://doi.org/10.1039/d5sc06282a.

Acknowledgements

References

1 C. Gao, F. Lyu and Y. Yin, *Chem. Rev.*, 2021, **121**, 834–881.

2 C. Xie, Z. Niu, D. Kim, M. Li and P. Yang, *Chem. Rev.*, 2020, **120**, 1184–1249.

3 Z. Li, S. Ji, Y. Liu, X. Cao, S. Tian, Y. Chen, Z. Niu and Y. Li, *Chem. Rev.*, 2020, **120**, 623–682.

4 D. Leybo, U. J. Etim, M. Monai, S. R. Bare, Z. Zhong and C. Vogt, *Chem. Soc. Rev.*, 2024, **53**, 10450–10490.

5 L. Liu and A. Corma, *Chem. Rev.*, 2023, **123**, 4855–4933.

6 J. D. Lee, J. B. Miller, A. V. Shneidman, L. Sun, J. F. Weaver, J. Aizenberg, J. Biener, J. A. Boscoboinik, A. C. Foucher, A. I. Frenkel, J. E. S. van der Hoeven, B. Kozinsky, N. Marcella, M. M. Montemore, H. T. Ngan, C. R. O'Connor, C. J. Owen, D. J. Stacchiola, E. A. Stach, R. J. Madix, P. Sautet and C. M. Friend, *Chem. Rev.*, 2022, **122**, 8758–8808.

7 Y. Kang, S. M. João, R. Lin, K. Liu, L. Zhu, J. Fu, W.-C. Cheong, S. Lee, K. Frank and B. Nickel, *Nat. Commun.*, 2024, **15**, 3923.

8 C. Xie, D. Yan, H. Li, S. Du, W. Chen, Y. Wang, Y. Zou, R. Chen and S. Wang, *ACS Catal.*, 2020, **10**, 11082–11098.

9 Y. Du, H. Sheng, D. Astruc and M. Zhu, *Chem. Rev.*, 2020, **120**, 526–622.

10 R. Jin, G. Li, S. Sharma, Y. Li and X. Du, *Chem. Rev.*, 2021, **121**, 567–648.

11 Z.-J. Guan, J.-J. Li, F. Hu and Q.-M. Wang, *Angew. Chem., Int. Ed.*, 2022, **61**, e202209725.

12 K. Xiao, Y. Xue, B. Yang and L. Zhao, *CCS Chem.*, 2021, **3**, 555–565.

13 W.-D. Tian, W.-D. Si, S. Havenridge, C. Zhang, Z. Wang, C. M. Aikens, C.-H. Tung and D. Sun, *Sci. Bull.*, 2024, **69**, 40–48.

14 W.-D. Si, C. Zhang, M. Zhou, W.-D. Tian, Z. Wang, Q. Hu, K.-P. Song, L. Feng, X.-Q. Huang, Z.-Y. Gao, C.-H. Tung and D. Sun, *Sci. Adv.*, 2023, **9**, eadg3587.

15 W.-D. Si, C. Zhang, M. Zhou, Z. Wang, L. Feng, C.-H. Tung and D. Sun, *Sci. Adv.*, 2024, **10**, eadm6928.

16 S.-S. Zhang, L. Feng, R. D. Senanayake, C. M. Aikens, X.-P. Wang, Q.-Q. Zhao, C.-H. Tung and D. Sun, *Chem. Sci.*, 2018, **9**, 1251–1258.

17 Y. Li, T. Higaki, X. Du and R. Jin, *Adv. Mater.*, 2020, **32**, 1905488.

18 Y. Li, M. Zhou and R. Jin, *Adv. Mater.*, 2021, **33**, 2006591.

19 B. Zhang, J. Chen, Y. Cao, O. J. H. Chai and J. Xie, *Small*, 2021, **17**, 2004381.

20 S. Li, X. Du, Z. Liu, Y. Li, Y. Shao and R. Jin, *Precis. Chem.*, 2023, **1**, 14–28.

21 Y. Liu, H. Tsunoyama, T. Akita, S. Xie and T. Tsukuda, *ACS Catal.*, 2011, **1**, 2–6.

22 G. Li, D.-e. Jiang, S. Kumar, Y. Chen and R. Jin, *ACS Catal.*, 2014, **4**, 2463–2469.

23 Y. Sun, E. Wang, Y. Ren, K. Xiao, X. Liu, D. Yang, Y. Gao, W. Ding and Y. Zhu, *Adv. Funct. Mater.*, 2019, **29**, 1904242.

24 Y. Zhang, P. Song, T. Chen, X. Liu, T. Chen, Z. Wu, Y. Wang, J. Xie and W. Xu, *Proc. Natl. Acad. Sci. U. S. A.*, 2018, **115**, 10588.

25 G. Li, X. Sui, X. Cai, W. Hu, X. Liu, M. Chen and Y. Zhu, *Angew. Chem., Int. Ed.*, 2021, **60**, 10573–10576.

26 X. Liu, E. Wang, M. Zhou, Y. Wan, Y. Zhang, H. Liu, Y. Zhao, J. Li, Y. Gao and Y. Zhu, *Angew. Chem., Int. Ed.*, 2022, **61**, e202207685.

27 K. Kwak, W. Choi, Q. Tang, M. Kim, Y. Lee, D.-e. Jiang and D. Lee, *Nat. Commun.*, 2017, **8**, 14723.

28 Y. Liu, X. Chai, X. Cai, M. Chen, R. Jin, W. Ding and Y. Zhu, *Angew. Chem., Int. Ed.*, 2018, **57**, 9775–9779.

29 Y. Li, H. K. Kim, R. D. McGillicuddy, S.-L. Zheng, K. J. Anderton, G. J. Stec, J. Lee, D. Cui and J. A. Mason, *J. Am. Chem. Soc.*, 2023, **145**, 9304–9312.

30 S. Su, Y. Zhou, L. Xiong, S. Jin, Y. Du and M. Zhu, *Angew. Chem., Int. Ed.*, 2024, **57**, e202404629.

31 S. Masuda, H. Hirai, P. Zhao, S. Takano, M. Ehara and T. Tsukuda, *ACS Catal.*, 2024, **14**, 17123–17131.

32 X.-K. Wan, J.-Q. Jia, Z.-A. Nan and Q.-M. Wang, *Sci. Adv.*, 2017, **3**, e1701823.

33 Z. Liu, H. Tan, B. Li, Z. Hu, D.-e. Jiang, Q. Yao, L. Wang and J. Xie, *Nat. Commun.*, 2023, **14**, 3374.

34 M. Bodiuzzaman, K. Murugesan, P. Yuan, B. Maity, A. Sagadevan, N. Malenahalli H, S. Wang, P. Maity, M. F. Alotaibi, D.-e. Jiang, M. Abulikemu, O. F. Mohammed, L. Cavallo, M. Rueping and O. M. Bakr, *J. Am. Chem. Soc.*, 2024, **146**, 26994–27005.

35 Z. Liu, J. Chen, B. Li, D.-e. Jiang, L. Wang, Q. Yao and J. Xie, *J. Am. Chem. Soc.*, 2024, **146**, 11773–27005.

36 S. M. Han, M. Park, J. Kim and D. Lee, *Angew. Chem., Int. Ed.*, 2024, **63**, e202404387.

37 J. Chai, S. Yang, Y. Lv, H. Chong, H. Yu and M. Zhu, *Angew. Chem., Int. Ed.*, 2019, **58**, 15671–15674.

38 Y. Tan, G. Sun, T. Jiang, D. Liu, Q. Li, S. Yang, J. Chai, S. Gao, H. Yu and M. Zhu, *Angew. Chem., Int. Ed.*, 2024, **63**, e202317471.

39 J.-Q. Fan, Y. Li, W. W. Xu and M.-B. Li, *Angew. Chem., Int. Ed.*, 2025, **64**, e202413861.

40 X. Kang, Y. Li, M. Zhu and R. Jin, *Chem. Soc. Rev.*, 2020, **49**, 6443–6514.

41 H. Hirai, S. Takano, T. Nakashima, T. Iwasa, T. Taketsugu and T. Tsukuda, *Angew. Chem., Int. Ed.*, 2022, **134**, e202207290.

42 Z. Liu, M. Zhou, L. Luo, Y. Wang, E. Kahng and R. Jin, *J. Am. Chem. Soc.*, 2023, **145**, 19969–19981.

43 W.-Q. Shi, L. Zeng, R.-L. He, X.-S. Han, Z.-J. Guan, M. Zhou and Q.-M. Wang, *Science*, 2024, **383**, 326–330.

44 A. Pniakowska, K. K. Ramankutty, P. Obstarczyk, M. P. Bakulić, Ž. S. Maršić, V. Bonačić-Koutecký, T. Bürgi and J. Olesiak-Bańska, *Angew. Chem., Int. Ed.*, 2022, **61**, e202209645.

45 S. Zhuang, D. Chen, L. Liao, Y. Zhao, N. Xia, W. Zhang, C. Wang, J. Yang and Z. Wu, *Angew. Chem., Int. Ed.*, 2020, **59**, 3073–3077.

46 Y. Tan, Y. Lv, L. Xu, Q. Li, J. Chai, S. Yang, H. Yu and M. Zhu, *J. Am. Chem. Soc.*, 2023, **145**, 4238–4245.

47 Q. Li, K. J. Lambright, M. G. Taylor, K. Kirschbaum, T.-Y. Luo, J. Zhao, G. Mpourmpakis, S. Mokashi-Punekar, N. L. Rosi and R. Jin, *J. Am. Chem. Soc.*, 2017, **139**, 17779–17782.

48 W. Zhang, S. Zhuang, L. Liao, H. Dong, N. Xia, J. Li, H. Deng and Z. Wu, *Inorg. Chem.*, 2019, **58**, 5388–5392.

49 X. Liu, G. Yao, X. Cheng, J. Xu, X. Cai, W. Hu, W. W. Xu, C. Zhang and Y. Zhu, *Chem. Sci.*, 2021, **12**, 3290–3294.

50 L. Xu, Q. Li, T. Li, J. Chai, S. Yang and M. Zhu, *Inorg. Chem. Front.*, 2021, **8**, 4820–4827.

51 J.-Q. Fan, Y. Yang, C.-B. Tao and M.-B. Li, *Angew. Chem., Int. Ed.*, 2023, **62**, e202215741.

52 Q. Li, S. Yang, T. Chen, S. Jin, J. Chai, H. Zhang and M. Zhu, *Nanoscale*, 2020, **12**, 23694–23699.

53 S. Yang, S. Chen, L. Xiong, C. Liu, H. Yu, S. Wang, N. L. Rosi, Y. Pei and M. Zhu, *J. Am. Chem. Soc.*, 2018, **140**, 10988–10994.

54 (*a*) Q. Li, T. Jiang, S. Yang, J. Chai, H. Yu and M. Zhu, CCDC 2374164: Experimental Crystal Structure Determination, 2025, DOI: **10.5517/ccdc.csd.cc2kphyq**; (*b*) Q. Li, T. Jiang, S. Yang, J. Chai, H. Yu and M. Zhu, CCDC 2128986: Experimental Crystal Structure Determination, 2025, DOI: **10.5517/ccdc.csd.cc29gcz4**; (*c*) Q. Li, T. Jiang, S. Yang, J. Chai, H. Yu and M. Zhu, CCDC 2341165: Experimental Crystal Structure Determination, 2025, DOI: **10.25505/fiz.icsd.cc2jl5gs**.